Accepted Manuscript

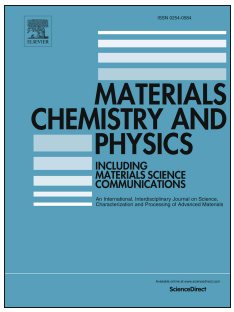

Thickness determination of ultrathin Poly(acrylic acid) shell on γ-Fe_2O_3 nanocore via small-angle scattering

Huailiang Li, Kunzhou Wang, Xianguo Tuo, László Almásy, Qiang Tian, Guangai Sun, Mark Julian Henderson, Qintang Li, András Wacha, Jérémie Courtois, Minhao Yan

PII: S0254-0584(17)30836-2

DOI: 10.1016/j.matchemphys.2017.10.047

Reference: MAC 20086

To appear in: *Materials Chemistry and Physics*

Received Date: 27 June 2017

Revised Date: 16 October 2017

Accepted Date: 17 October 2017

Please cite this article as: H. Li, K. Wang, X. Tuo, Láó. Almásy, Q. Tian, G. Sun, M.J. Henderson, Q. Li, Andrá. Wacha, Jéé. Courtois, M. Yan, Thickness determination of ultrathin Poly(acrylic acid) shell on γ-Fe_2O_3 nanocore via small-angle scattering, *Materials Chemistry and Physics* (2017), doi: 10.1016/j.matchemphys.2017.10.047.

This is a PDF file of an unedited manuscript that has been accepted for publication. As a service to our customers we are providing this early version of the manuscript. The manuscript will undergo copyediting, typesetting, and review of the resulting proof before it is published in its final form. Please note that during the production process errors may be discovered which could affect the content, and all legal disclaimers that apply to the journal pertain.

Graphical abstract

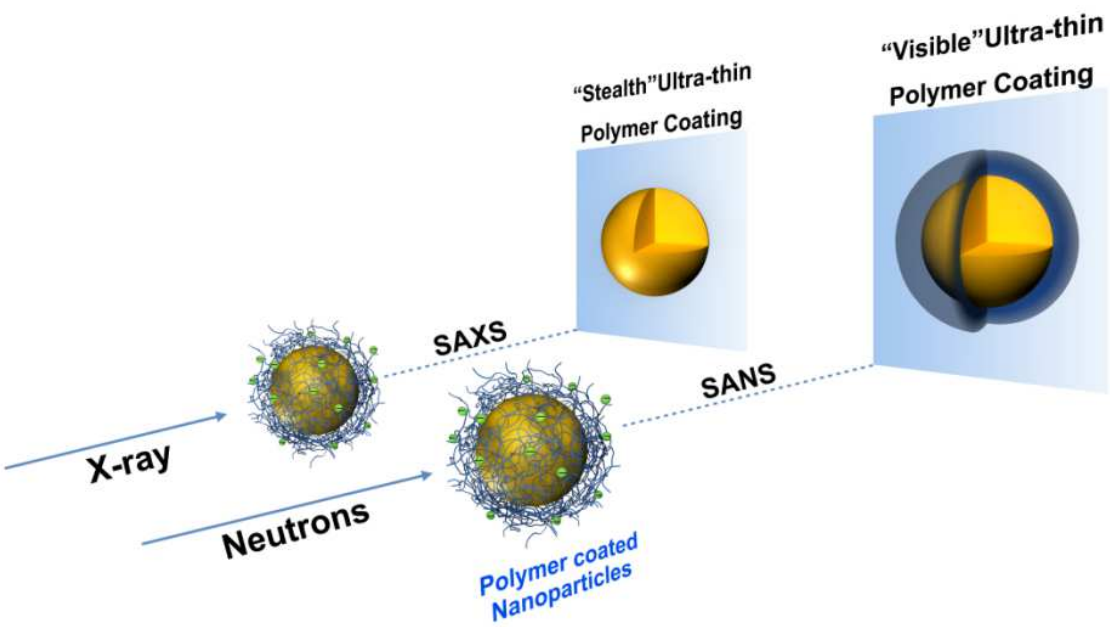

ACCEPTED MANUSCRIPT

Thickness Determination of Ultrathin Poly(acrylic acid) Shell on γ-Fe_2O_3 Nanocore via Small-Angle Scattering

Huailiang Li[1,2,⊥], Kunzhou Wang[1,⊥], Xianguo Tuo[2], László Almásy[1,3], Qiang Tian[4], Guangai Sun[4], Mark Julian Henderson[,1], Qintang Li[1], András Wacha[5], Jérémie Courtois[,1] and Minhao Yan[*,1]*

1 State Key Laboratory Cultivation Base for Nonmetal Composites and Functional Materials, Southwest University of Science and Technology, Mianyang 621010, China

2 Sichuan University of Science and Engineering, Zigong 643000, China.

3 Wigner Research Centre for Physics, POB 49, Budapest, 1525, Hungary

4 Key Laboratory of Neutron Physics and Institute of Nuclear Physics and Chemistry, China Academy of Engineering Physics (CAEP), Mianyang 621999, China

5 Biological Nanochemistry Research Group, Institute of Materials and Environmental Chemistry, Research Centre for Natural Sciences, Hungarian Academy of Sciences, Magyar tudósok körútja 2, 1117 Budapest, Hungary

⊥ H. L and K. W contributed equally to this work.

* to whom correspondence should be addressed:
Prof. Yan Minhao and Prof. Mark Julian Henderson
State Key Laboratory Cultivation Base for Nonmetal Composites and Functional Materials
Southwest University of Science and Technology (SWUST),
Mianyang
621010
P. R. China
Tel : 008613778092806
Email : yanminhao@swust.edu.cn and mark_henderson@swust.edu.cn

ACCEPTED MANUSCRIPT

Abstract

Core-shell polymer coated superparamagnetic nanoparticles are critical tools in bio-nanotechnology, in which the soft and thin polymeric coatings play a key role in their stabilization, surface functionality and biocompatibility. Standard characterization tools, such as Transmission Electron Microscopy are indispensable for the morphological characterization of the metal-containing core but they cannot clearly discriminate between core and shell components. Dynamic Light Scattering can only overestimate the shell thickness by measuring the particle hydrodynamic diameter. Here, we describe Small-Angle X-ray Scattering and Small-Angle Neutron Scattering as tools to study poly (acrylic) acid coated gamma iron oxide superparamagnetic nanoparticles dispersed in aqueous medium. Our results show that Small-Angle Scattering techniques offers in situ and sensitive measurements of the "stealth" polymer coatings which cannot be accurately detected by other techniques. The Small Angle Scattering approach presented in this work is applicable for analysis of core-shell organic/inorganic hybrid nanoparticles systems for a broad range of applications.

Keywords: Core-Shell nanoparticles, Ultra-thin Polymer coatings, Small-Angle X-ray and Neutron Scattering

ACCEPTED MANUSCRIPT

1. Introduction

Iron oxide nanoparticles (NPs) (< 10 nm) have utility in several biomedical applications including imaging, separation, targeting and hyperthermia[1-6]. The nanometric size of these particles allows them to diffuse deeply through tissue[4] and ensures their superparamagnetic behavior[7]. However, the integration of these contrast agents into living systems remains incomplete because they are easily recognized as foreign bodies by the reticuloendothelial system (**RES**; spleen, liver, bone marrow, macrophages) and opsonin proteins. This decreases the effective concentration of the NPs in vivo with diminished targeting capabilities. In this paper we describe a method based on small-angle scattering from individual NPs colloids in aqueous media –which are the most frequently applied in vivo– to obtain the structural features of the ultrathin polymer stealth shell.

A variety of cloaking strategies have been developed to shield these particles from RES recognition and subsequently increase in vivo circulation times. NPs are frequently coated with biocompatible macromolecules such as polyethylene glycol (PEG) to increase their stability and the half-life of blood circulation[8]. Another novel approach produces nanoparticles coated with a lysed cell membrane to prevent recognition[9]. Regardless of the exact approach, the overall goal is to increase colloidal stability and circulation time to facilitate nanoparticle imaging or therapy.

A more recent development is composite NPs that also offer good stability in biological tissues and a long half-life[10]. These organic/inorganic composite NPs have attracted significant attention and have been extensively studied by physicists, chemists and biologists[11-13]. However, careful in situ characterization of the organic corona surrounding these hybrid materials is largely incomplete. Such information would offer important details about the

interface between the solvent/organic layer and organic layer/inorganic particle surface to ultimately improve the utility of these materials.

Detailed characterization of the core and shell is critical to the development of composite NPs. Fourier Transform infrared spectroscopy (FTIR), Dynamic Light Scattering (DLS) and X-ray scattering are the most commonly used tools to obtain structural information on organic/inorganic hybrid colloidal NPs, however, these techniques provide details about the presence of the organic composite, the total hydrated radius and average core size, respectively, and they usually cannot discriminate between the core and shell[14-21]. Small-Angle Scattering technique is a powerful tool to study the size, shape and internal structure of organic and inorganic colloids in the size range of 1−200 nm. One fundamental prerequisite for the use of Small-Angle X-ray Scattering (SAXS) on particles in solution is the existence of a sufficiently high contrast in electronic density between the solvent and the dispersed particle, or part of the particle. While for the metal-containing core the contrast is strongly due to the relatively heavy elements, the scattering length densities of the hydrocarbon polymer shell and the solvent are often similar, leading to a low contrast especially for strongly solvated shells/brushes in water. Usually, because of the low grafting density of the polymer, and consequently the low shell-to-solvent contrast, the shell is not visible enough to reveal its morphology directly[22]. An elegant exception is where iron oxide core−poly(ethylene glycol) brush shell nanoparticles having extremely high polymer grafting density was investigated using small-angle X-ray scattering (SAXS)[23]. In this particular case, uniquely high polymer grafting densities enabled the characterization of the associated density profiles possible by increasing the scattering length density contrast. Although, Transmission Electron Microscopy (TEM) is a powerful and accurate

technique, in most cases it can easily visualize the electron-dense core [24] but not the organic shell composed of light elements (C and H).

On the other hand, the scattering length of nuclei varies randomly across the periodic table and also between isotopes of the same element. A useful example of this is hydrogen (^{1}H) and deuterium (^{2}H). In combination with neutron contrast variation, i.e. replacing isotopes of the same element, Small-Angle Neutron Scattering (SANS) can reveal more structural information of organic/inorganic hybrid system with the combination of SAXS[25-27].

Contrast variation SANS data and SAXS data was presented by Vroege *et al.*, for oleic acid-coated magnetic iron particles, which underwent partial oxidation of the particle surface, exhibiting a core–inner shell–outer shell structure[28]. More recently, Unruh *et al.* studied stabilizer layer of ZnO NPs prepared in a wet chemical synthesis from zinc acetate. By using a combined SAXS/SANS approach, they demonstrated the existence of an enhanced acetate anion concentration within a thin shell surrounding the ZnO NPs, and the acetate distribution could be quantitatively determined[29].

Usually the organic polymer coating contains large amounts of hydrogen. By exploiting the different scattering amplitudes of hydrogen and deuterium, the combination of SANS and deuteration methods offers a unique advantage for the investigation of organic/inorganic nanocomposite. Jestin *et al.* studied the linear fractal aggregates of 3–4 native γ-Fe_2O_3 nanoparticles grafted with polystyrene (PS) chains in dimethylacetamide (DMAc) by using SANS and SAXS. The behavior of the grafted PS chains was found to be in agreement with scaling laws derived for brushes in a theta solvent[30]. Hore *et al.* studied the structure of deuterated poly (methyl methacrylate) (d-PMMA) nanocomposites containing PMMA-grafted Fe_3O_4 nanospheres. A combination of SANS measurements and self-consistent field theory

(SCFT) calculations allowed the conformation of the PMMA brush chains to be studied[31]. Berret *et al.* studied water-soluble clusters made from 7 nm γ-Fe_2O_3 nanoparticles by SANS. The internal structure factor of the clusters was derived and exhibited a universal behavior[21]. However, it is somewhat surprising that SANS is rarely used to study individual NPs colloids with ultrathin polymer coatings in aqueous media which are the most frequently used in various applications.

In this work, we synthesized highly stable, 5 nm and 7 nm colloidal γ-Fe_2O_3 superparamagnetic NPs suitable for small-angle scattering technique. We then coated γ-Fe_2O_3 NPs with polyacrylic acid (PAA) which offers remarkable colloidal stability (over years) and free carboxyl groups as reactive for subsequent bio functionalization. Using SAXS and SANS measurements, the core and shell of dispersed nanoparticles were probed with the aim to determine the thickness of the ultra-thin polymer corona in the colloidal state. The present work demonstrates a direct, nondestructive and in-situ observation method of ultra-thin PAA coating in aqueous media, which cannot be easily achieved by other techniques. The results will offer important insights for researchers studying composite NPs with ultra-thin organic coatings.

2. Materials and Methods

2.1 Materials

$FeCl_2 \cdot 4H_2O$, $FeCl_3 \cdot 6H_2O$, $Fe(NO)_3 \cdot 9H_2O$, ammonia (20 wt. % in water), nitric acid (52 wt. % in water), acetone, diethyl ether; poly(acrylic acid) with M_W = 2100 g. mol^{-1} and 5000 g. mol^{-1} were obtained from Sigma Aldrich and used as received. All the water used in the study was MilliQ quality water (Millipore®). Deuterium Oxide (D_2O with D content 99.9%) was obtained from Cambridge Isotope Laboratories, Inc.

2.2 Synthesis of nanoparticles

Poly (acrylic acid)-coated iron oxide NPs were prepared following well-established method from literature. Maghemite (γ-Fe_2O_3) nanocrystals were synthesized by the Massart method[32]. Briefly, iron (II) and iron (III) salts are co-precipitated in an alkaline aqueous media at room temperature. The resulting magnetite (Fe_3O_4) nanocrystals are then transferred to an acidic aqueous medium using nitric acid and oxidized into maghemite by addition of $Fe_3(NO_3)_3$ with boiling solvent, which leads to the oxidation of the $Fe^{II}O$ of magnetite Fe_3O_4 into stable γ-$Fe_2^{III}O_3$ maghemite nanoparticles. The crystalline structure of the maghemite nanoparticles is revealed by Electron Diffraction. The diffraction pattern is presented in Supporting Information S1. Vibrating sample magnetometry (VSM) measurements of a liquid dispersion of γ-Fe_2O_3 reveals their superparamagnetic behavior at T = 25 ºC with saturation magnetization of 46.2 emu. g^{-1} (Supporting Information S2). The synthesis gave maghemite nanoparticles with a broad distribution of sizes. The distribution is generally found to be lognormal, with an average diameter around 10 nm and a polydispersity around 0.4. The polydispersity index is defined as the ratio between the standard deviation and the average diameter[33].

Size sorting was used to reduce the polydispersity of γ-Fe_2O_3 NPs using successive liquid-liquid phase separations induced by the addition of nitric acid[34]. Adding large amount of nitric acid both decreased the pH from 2 to 0.5 and simultaneously increased the ionic strength. The phase separation is of the liquid-gas type, and the more concentrated phase was separated by magnetic sedimentation: the concentrated phase was called “C”, and the diluted phase “S”, (for supernatant). Moreover, as shown in Refs. [32, 35], the concentrated phase contained the largest particles, whereas the diluted phase contains the smallest ones. The flocculated particles of the

concentrated phase “C” were then redispersed by adding water (which increases the pH from 0.5 to 1.8 and decreases the ionic strength by dilution of species). The phase “S” contains dispersed particles, and counterions (especially nitrate, NO_3^-) which have to be removed. In this way, the γ-Fe_2O_3 NPs from the synthesis have been firstly sorted in two batches: “C” and “S”, containing respectively “the largest” and the “smallest” particles. The process of sorting using phase separation can be repeated on “C”, leading to C1C and C1S, and on “S” leading to “S1C” and “S1S”, etc. At the end, two batches of γ-Fe_2O_3 nanocrystals with nominal diameters of 5 nm (denoted NP1) and of 7 nm (denoted NP2) suspended in acidic aqueous media (pH 1.8) have been obtained.

Second, the bare NPs were coated in acidic environment with PAA oligomers with two molecular weights of 2100 $g \cdot mol^{-1}$ and 5000 $g \cdot mol^{-1}$ using the precipitation-redispersion process[36]. The drop-by-drop addition of a solution of PAA at pH = 1.8 to a dispersion of bare NPs at pH = 1.8 leads to precipitation of the nanocrystals and their adsorbed polymer chains. For both PAA_{2k} and PAA_{5k}, the mass ratio between added PAA and bare NPs were 10 : 1 in order to archive the saturated coating effect. Single particles were then recovered by redispersion at pH = 10 with adding NH_4OH. The dispersions of PAA coated NPs were finally purified by dialysis in deionized water with removing the excess of un-coated PAA and other impurities. The coating process is illustrated in Scheme 1. The resulted PAA_{2K}-coated NPs (denoted NP1-PAA_{2K} and NP2-PAA_{2K}) and PAA_{5K}-coated NPs (denoted NP1-PAA_{5K} and NP2-PAA_{5K}) were stored in neutral aqueous media (in either H_2O or D_2O at pH 7.5). The stability and resilience of the poly(acrylic acid) coating have been investigated previously[16]. These results confirm the existence of a highly resilient PAA adlayer onto the γ-Fe_2O_3 nanoparticles, a property that is crucial for applications.

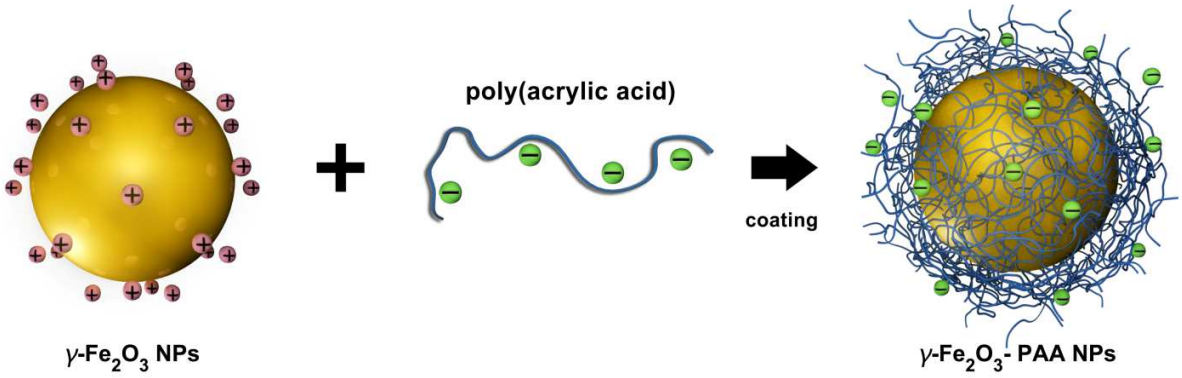

Scheme 1. *Representation of the coating process using positively charged bare NPs and negatively charged PAA oligomers. Synthesized γ-Fe_2O_3-PAA NPs exhibit negative charges at their surface at pH = 7.5.*

2.3 Characterization

Dynamic light scattering (DLS) was monitored on a Multi-angle particle size and zeta potential analyzer (Brookhaven NanoBrook Omni).

Transmission electron microscopy (TEM) was carried out on Zeiss Libra200FE at the Analysis and Characterization Center of Southwest University of Science and Technology.

The X-ray scattering measurements were performed by a SAXSpace small angle X-ray scattering instrument (Anton Paar, Austria, Cu-Kα, λ = 0.154 nm), equipped with a Kratky block-collimation system and an image plate (IP) as the detector. The X-ray generator was operated at 40 kV and 50 mA. A standard temperature control unit (Anton-Paar TCS 150) connected with the SAXSpace was used to control the temperature at 25 ºC. Samples were transferred to thin-wall quartz capillary with inner diameter of 1 mm. For colloidal NPs samples with different concentrations and different size, different exposure times from 5 min to 60 min

were used in order to give a good signal-to-noise ratio. The scattering curve of pure D_2O filled in the same capillary was recorded as the background with exposure time of 1 hour. All the data were corrected for transmission and background scattering from the capillary and D_2O according to the scattering of D_2O in the wide-angle region.

The SANS measurements have been performed on the Yellow Submarine small-angle neutron scattering instrument installed at the cold neutron beamline of the 10MW steady-state research reactor of the Budapest Neutron Centre (BNC), Hungary. The monochromatic beam with a mean wavelength of 0.49 nm and 0.2 FWHM was produced by a mechanical velocity selector. BF_3 gas filled multiwire detector of 64cm × 64cm sensitive area was placed at distances of 5.5 m and 1.35 m from the sample, to cover the q-interval of 0.08-2 nm^{-1}. The measurements were performed at room temperature. The preliminary SANS tests were conducted on Suanni SANS instrument installed at CMRR, Mianyang, China[37]. By considering the X-ray and neutron scattering length density contrast between γ-Fe_2O_3, PAA and outer solvent (details shown in Supporting Information S1), D_2O was chosen as the solvent for both bare and coated NPs dispersions for SAXS and SANS experiments.

3. Results and Discussion

3.1 TEM characterization of bare and coated γ-Fe_2O_3 NPs

For NP1, TEM images (Figures 1 a, b, c) of both bare and coated NPs demonstrate that the particles were individually dispersed without agglomeration before and after polymer coating. In the case of coated NPs (Figure 1 b,c), the no-contact positioning of the particles on the dry grid indirectly prove that the coated polymer uniformly attached the surface of particles. Nevertheless, the outer organic layer cannot be revealed because their electronic density is too low to produce

contrast. In each of the three cases (NP1, NP1-PAA_{2K} and NP1-PAA_{5K}), a series of TEM images similar to those shown in Figures 1 were quantitatively analyzed to retrieve the size distribution histogram, and fitted by a log-normal distribution function (Supporting Information S2) [31]. In order to get good statistic, more than 250 nanoparticles with clear edge from different area in TEM sample grid were selected for measurement and account. The median diameter D_{TEM} of NP1, NP1-PAA_{2K} and NP1-PAA_{5K} are 4.9 ± 0.1 nm, 5.0 ± 0.1 nm and 5.1 ± 0.1 nm respectively, with polydispersity S_{TEM} all equal to 0.18 ± 0.03.

For NP2, the difference between bare and coated NPs can hardly be detected by TEM neither (Supporting Information S3). The D_{TEM} of NP2, NP2-PAA_{2K} and NP2-PAA_{5K} are 7.2 ± 0.1 nm, 7.3 ± 0.1 nm and 7.4 ± 0.1 nm respectively, with S_{TEM} all equal to 0.28 ± 0.03. The results of analysis of TEM measurements are listed in Figure 1d. These data allow to conclude about some details of the coating process. First, the bare and coated particles have essentially the same size, an indication that the coating process was not selective to the particle size, and did not cause any appreciable enlargement of the mean particle diameter. Second, the polydispersity of the larger particles was higher, 0.28 compared to 0.18, a result of the size sorting procedure. The typical size distribution for particles prepared by co-precipitation and without sorting would be about 0.40. Finally, it is seen that TEM method is insufficient to characterize the ultra-thin polymer layer around the inorganic NPs.

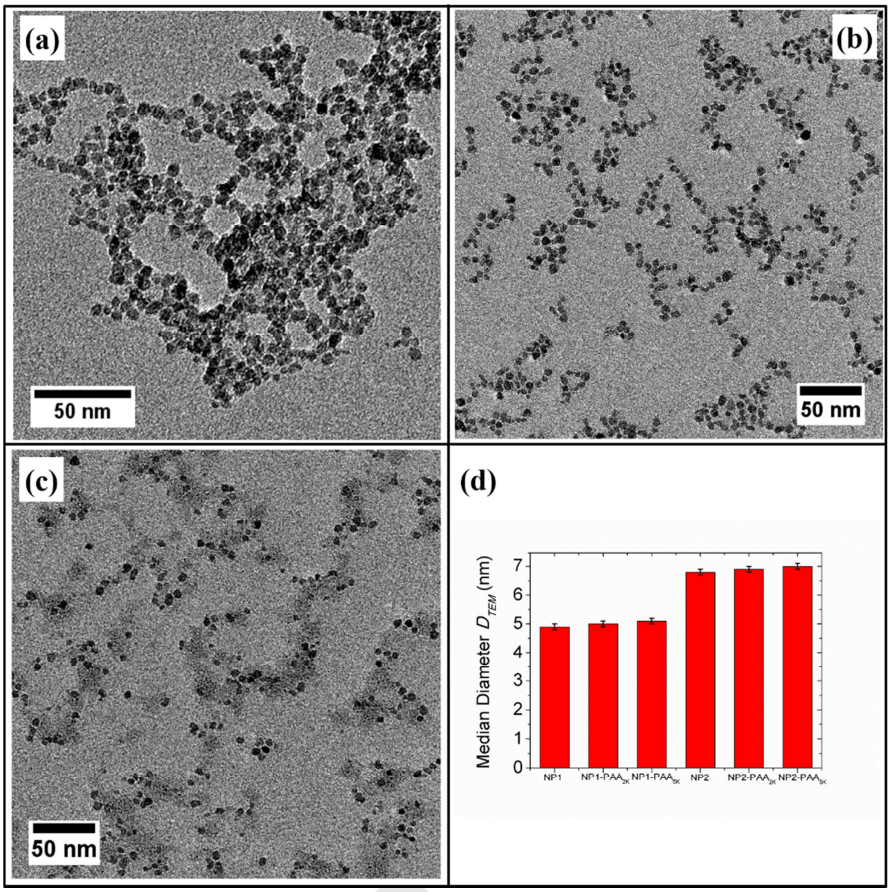

Figure 1. *Transmission electron micrographs of bare and coated NP1. (a) Bare NP1; (b) NP1 coated with PAA_{2K} (NP1-PAA_{2K}); (c) NP1 coated with PAA_{5K} (NP1-PAA_{5K}); (d) Median diameter of bare and coated NPs obtained from TEM.*

3.2 DLS characterization of bare and polymer coated γ-Fe_2O_3 NPs

The γ-Fe_2O_3 NPs prepared by co-precipitation are stabilized in acidic aqueous media (pH 1.8) by electrostatic repulsion due to surface-bound protons (Scheme 1). DLS measurements reveal hydrodynamic diameters D_H of bare NP1 and NP2 to be 8.4 nm and 20.2 nm, and their zeta potential were found to be +19 mV and +21 mV respectively (Table 1). The positive surface charges ensure the colloidal stability of bare NPs[38]. However, their highly acidic storage

environment is not consistent with an *in vivo* environment, i.e., the particle surface needs to be functionalized to realize biocompatibility and further functionality. Therefore, we used a "precipitation-redispersion" method to coat nanoparticle surface with 2100 g. mol^{-1} and 5000 g. mol^{-1} PAA (Scheme 1). Because of the electrostatic repulsion induced from the carboxyl groups attached on the PAA backbones as well as the steric repulsion introduced by the polymer chains, these polymer coated γ-Fe_2O_3 nanocrystals exhibit remarkable colloidal stability in aqueous media. Their corresponding D_H remain stable over years in neutral aqueous media (pH 7.5). The large number of free carboxyl groups around the NPs could facilitate further biological functionalization. The D_H and zeta potential of coated NPs are listed in Table 1. The relevant negative surface charge and the evident difference of D_H between bare and coated NPs directly prove the existence of the polymer layer. Using the DLS technique, we estimate that the hydrodynamic sizes of polymer coating are about 7 nm and 10 nm for the coating made from PAA_{2K} and PAA_{5K} respectively. Higher zeta potential from bigger molecular weight indicates that the coating made from PAA_{5k} should have higher charge density than that made from PAA_{2k}. Beyond this useful information, the DLS technique still cannot precisely measure the coating thickness in aqueous media.

Table 1. *Size and zeta potentials of bare and coated NPs characterized from DLS*

Sample name	D_H (nm)	Polydispersity S_{DLS}	Hydrodynamic size of polymer coating (nm)	zeta potential (mv)
NP1	8.4	0.18	—	+ 19
NP1-PAA_{2K}	22.0	0.21	6.8	- 29
NP1-PAA_{5K}	28.0	0.25	9.8	- 33
NP2	20.2	0.25	—	+ 21
NP2-PAA_{2K}	34.0	0.23	6.9	- 32
NP2-PAA_{5K}	43.3	0.24	11.5	- 34

3.3 SAXS characterization of bare and polymer coated NPs

Suspensions of bare and coated NPs in D_2O were characterized by the SAXS method. As the SAXS curves obtained from bare and coated particles, shown in Figures 2, almost superimpose, the curves of coated samples have been offset for clarity.

A core-shell sphere model with a lognormal distribution of core size was used to fit the scattering curves (model description is shown in Supporting Information S4) and the results are compiled in Table 2. The contrast between the polymer shell and the solvent is negligible compared to the core-solvent contrast, therefore the shell thickness had been fixed to 1 nm. Varying this value within a reasonable range did not change appreciably the resulting core size. SAXS provided data with higher statistical accuracy compared to TEM in terms of size characterization but was not sensitive to the organic corona surrounding core because of the low electron density contrast between the organic layer and the surrounding solvent (shown in Table S1).

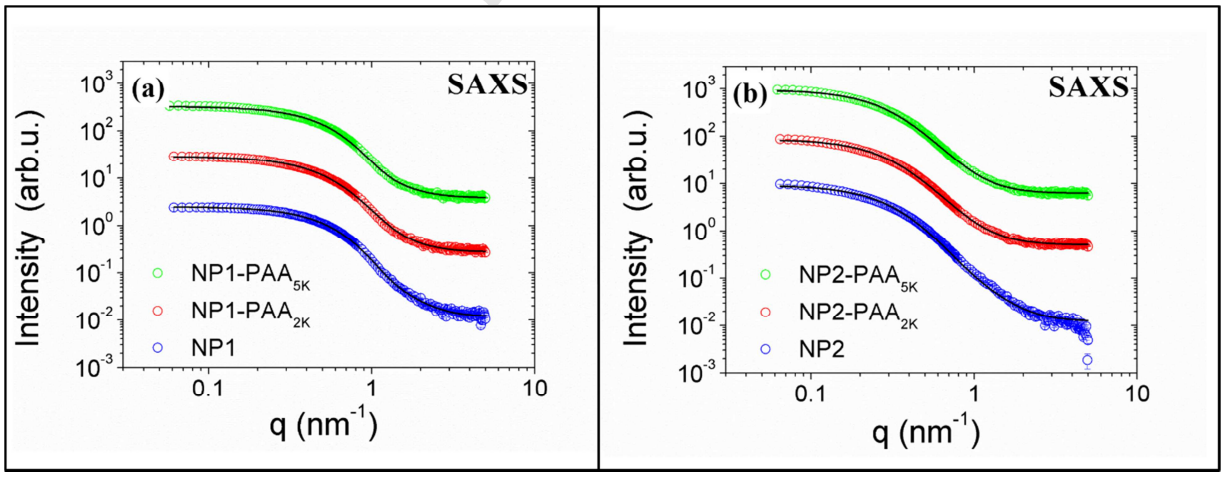

Figures 2. *SAXS data of γ-Fe_2O_3 nanoparticles suspensions. (a) NP1 without and with PAA coating. (b) NP2 without and with PAA coating. The data are rescaled vertically. The continuous lines are best fits to log-normal size distribution of spherical particles.*

Table 2. *Results of SAXS and SANS analysis on bare and coated NPs*

Sample	Fitted core radius R_{SAXS} (nm)	Polydispersity S_{SAXS}	Fitted core radius R_{SANS} (nm)	Shell thickness $D_{shell\ SANS}$ (nm)
NP1	2.43 ± 0.02	0.31	2.56 ± 0.01	-
NP1-PAA_{2K}	2.50 ± 0.02	0.35	2.56 (fixed)	1.246±0.002
NP1-PAA_{5K}	2.48 ± 0.02	0.30	2.56 (fixed)	1.320±0.002
NP2	3.92 ± 0.02	0.27	3.86 ± 0.01	-
NP2-PAA_{2K}	3.91 ± 0.01	0.34	3.86 (fixed)	1.244±0.003
NP2-PAA_{5K}	4.40 ± 0.01	0.39	3.86 (fixed)	1.323±0.003

3.4 SANS characterization of bare and coated NPs

SANS measurements were performed in D_2O suspensions of bare and coated NPs. The role of D_2O was to enhance the scattering from the polymer shell, due to its high contrast both to iron oxide, and D_2O (Table S1). Different with SAXS data, the SANS curves from coated NPs present higher absolute intensity than the one from bare NPs (shown in Figures 3). Moreover the coating made from higher molecular weight give higher intensity than the ones from lower molecular weight. This indicates that SANS technique is powerful to discover the ultra-thin organic coating around individual NPs of colloidal dimensions.

A linear contrast profile within the PAA shell has been assumed according to the experimental coating process (Scheme 2). The data were fitted by SASfit software [39], and the *q*-resolution was taken into account by convolving the theoretical curve with the instrument

resolution function. The description of the core-shell scattering model is given in the Supporting Information S4.

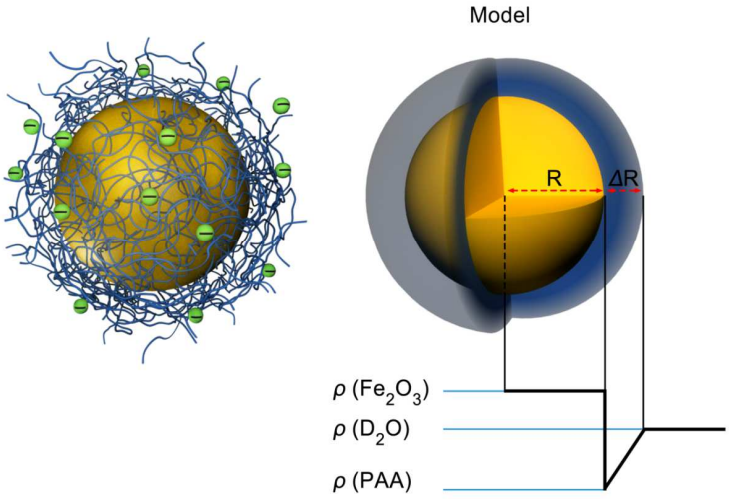

Scheme 2. *Left: Representation of the polymer coated NPs. Right: the sphere model used to analyze SANS data for the iron oxide composite materials. Here the core is shown in yellow and the shell (ΔR) is blue. The scattering length density ρ of D_2O, pure PAA shell and γ-Fe_2O_3 are 6.63×10^{10} cm^{-2}, 1.59×10^{10} cm^{-2} and 7.17×10^{10} cm^{-2} respectively.*

First, the SANS data of the bare NP1 and NP2 colloidal suspensions have been analyzed. The size distribution has been fixed at σ = 0.4, and the mean radius R was fitted together with scaling and background parameters. The fitted radii are found in good arrangement with the ones obtained from SAXS, indicating the reliability of the both techniques.

Next, the organic shell thickness were fitted by keeping the mean core size fixed. Using the known scattering length densities for the core, the polymer and the solvent, Δ*R* was the only structure variable. The SANS fitting results are compiled in Table 2. The results show the existence of the thin polymer coating, its maximal thickness within the linear profile

approximation was about 1.3±0.2 nm. γ-Fe_2O_3 particles covered with longer polymer chains give slightly larger extended volume. Although the difference obtained by fitting is within the estimated error range, it may indicate a trend that the polymer molecules are not covering tightly the particle surface. This is in agreement with the DLS results, showing explicitly that for the larger polymer, the extended chains capturing a large amount of hydration water are responsible for the strong increase of the hydrodynamic radius.

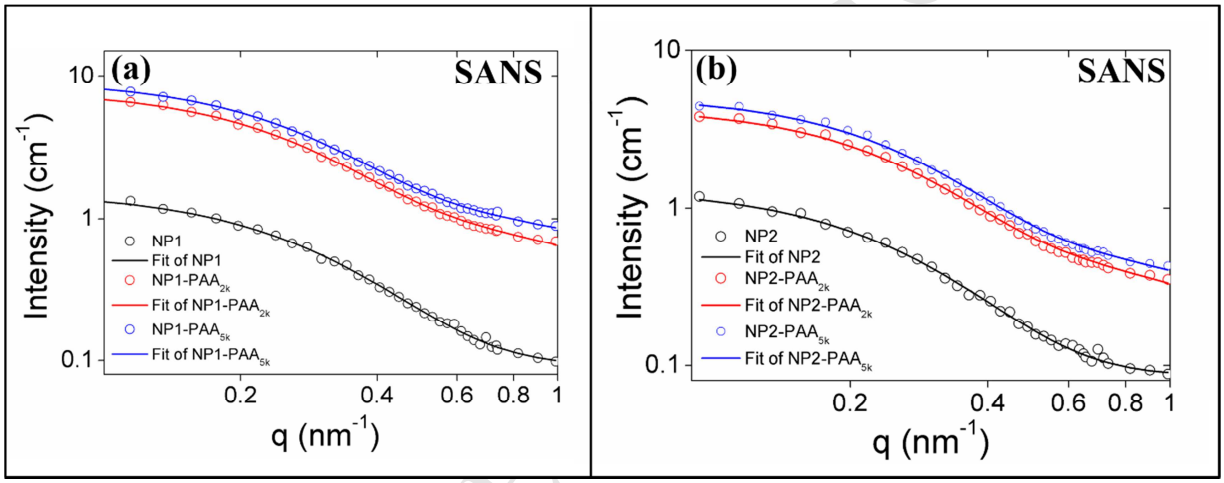

Figures 3. *SANS curves obtained from of (a) NP1 and their corresponding coated samples which are dispersed in D_2O; (b) NP2 and their corresponding coated samples. The continuous line is the best fit calculation using a log-normal distribution of bare NPs and a linear contrast profile of the organic shell for the coated NPs.*

4. Conclusions

Colloid suspensions of superparamagnetic NPs of different sizes and coated with organic polymer have been prepared and characterized with multiple methods. TEM measurements allowed direct visualization of the particles and quantitative size and size distribution data but

were insensitive to changes in the organic shell because of the low electron density of the PAA polymer. While DLS clearly showed a size increase after coating, this technique only measured the hydrodynamic radius and thus overestimated the size of the shell. SAXS offered statistically precise determination of the mean particle size, but could not discriminate between the coated and uncoated materials. However, small-angle scattering using neutron contrast variation could clearly confirm the presence of the PAA corona enabling the corona thickness to be determined. The combination of these techniques offer structural information on organic/inorganic (core/shell structure) superparamagnetic nanocomposite particles. Ultimately, we believe that SANS and SAXS methods will find widespread use in the biomedical community to characterize drug delivery vehicles and imaging contrast agents. The analysis methods demonstrated in this work are expected to be generally applicable for studying nano-composite colloidal systems with organic shells, which would provide a powerful guidance to practical applications.

Authors' information

Corresponding authors

yanminhao@swust.edu.cn and mark_henderson@swust.edu.cn

Author Contribution

⊥H. L and K. W contributed equally to this work.

Notes

The authors declare no competing financial interest.

Acknowledgement

ACCEPTED MANUSCRIPT

ACCEPTED MANUSCRIPT

This research was supported by Sichuan Province Education Department Innovation Team Foundation (16zd1104); Sichuan Province Science Foundation for Young Scientists (No. 15zs2111); Open Project of the Key Laboratory of Neutron Physics and Institute of Nuclear Physics and Chemistry, China Academy of Engineering Physics (No. 2014BB06); Open Project of State Key Laboratory Cultivation Base for Nonmetal Composites and Functional Materials (No. 11zxfk26) and by Research Funding from Southwest University of Science and Technology (No. 15zx7101 and 15zx7107).

ACCEPTED MANUSCRIPT

References

[1] P. Oswald, O. Clement, C. Chambon, E. Schouman-Claeys, G. Frija, Liver positive enhancement after injection of superparamagnetic nanoparticles: Respective role of circulating and uptaken particles, Magnetic Resonance Imaging, 15 (1997) 1025-1031.
[2] D.K. Kim, Y. Zhang, J. Kehr, T. Klason, B. Bjelke, M. Muhammed, Characterization and MRI study of surfactant-coated superparamagnetic nanoparticles administered into the rat brain, Journal of Magnetism and Magnetic Materials, 225 (2001) 256-261.
[3] I. Brigger, C. Dubernet, P. Couvreur, Nanoparticles in cancer therapy and diagnosis, Advanced Drug Delivery Reviews, 54 (2002) 631-651.
[4] C.C. Berry, Possible exploitation of magnetic nanoparticle-cell interaction for biomedical applications, Journal of Materials Chemistry, 15 (2005) 543-547.
[5] Y.-w. Jun, Y.-M. Huh, J.-s. Choi, J.-H. Lee, H.-T. Song, KimKim, S. Yoon, K.-S. Kim, J.-S. Shin, J.-S. Suh, J. Cheon, Nanoscale Size Effect of Magnetic Nanocrystals and Their Utilization for Cancer Diagnosis via Magnetic Resonance Imaging, Journal of the American Chemical Society, 127 (2005) 5732-5733.
[6] A.-H. Lu, E.L. Salabas, F. Schüth, Magnetic Nanoparticles: Synthesis, Protection, Functionalization, and Application, Angewandte Chemie International Edition, 46 (2007) 1222-1244.
[7] Q.A. Pankhurst, J. Connolly, S.K. Jones, J. Dobson, Applications of magnetic nanoparticles in biomedicine, Journal of Physics D: Applied Physics, 36 (2003) R167-R181.
[8] J.V. Jokerst, T. Lobovkina, R.N. Zare, S.S. Gambhir, Nanoparticle PEGylation for imaging and therapy, Nanomedicine, 6 (2011) 715-728.
[9] C.M.J. Hu, Z. Li, A. Santosh, C. Connie, R.H. Fang, Z. Liangfang, Erythrocyte membrane-camouflaged polymeric nanoparticles as a biomimetic delivery platform, Proceedings of the National Academy of Sciences of the United States of America, 108 (2011) 10980-10985.
[10] Y.-S. Lin, S.-H. Wu, Y. Hung, Y.-H. Chou, C. Chang, M.-L. Lin, C.-P. Tsai, C.-Y. Mou, Multifunctional Composite Nanoparticles: Magnetic, Luminescent, and Mesoporous, Chemistry of Materials, 18 (2006) 5170-5172.
[11] F. Zhang, E. Lees, F. Amin, P. Rivera_Gil, F. Yang, P. Mulvaney, W.J. Parak, Polymer-Coated Nanoparticles: A Universal Tool for Biolabelling Experiments, Small, 7 (2011) 3113-3127.
[12] C. Freese, M.I. Gibson, H.-A. Klok, R.E. Unger, C.J. Kirkpatrick, Size- and Coating-Dependent Uptake of Polymer-Coated Gold Nanoparticles in Primary Human Dermal Microvascular Endothelial Cells, Biomacromolecules, 13 (2012) 1533-1543.
[13] D. Hühn, K. Kantner, C. Geidel, S. Brandholt, I. De Cock, S.J.H. Soenen, P. Rivera_Gil, J.-M. Montenegro, K. Braeckmans, K. Müllen, G.U. Nienhaus, M. Klapper, W.J. Parak, Polymer-Coated Nanoparticles Interacting with Proteins and Cells: Focusing on the Sign of the Net Charge, ACS Nano, 7 (2013) 3253-3263.
[14] G. Utkan, F. Sayar, P. Batat, S. Ide, M. Kriechbaum, E. Pişkin, Synthesis and characterization of nanomagnetite particles and their polymer coated forms, Journal of Colloid and Interface Science, 353 (2011) 372-379.
[15] M. Yan, J. Fresnais, J.F. Berret, Growth mechanism of nanostructured superparamagnetic rods obtained by electrostatic co-assembly, Soft Matter, 6 (2010) 1997-2005.
[16] J. Fresnais, M. Yan, J. Courtois, T. Bostelmann, A. Bée, J.F. Berret, Poly(acrylic acid)-coated iron oxide nanoparticles: Quantitative evaluation of the coating properties and applications for the removal of a pollutant dye, Journal of Colloid and Interface Science, 395 (2013) 24-30.
[17] S. Fischer, A. Salcher, A. Kornowski, H. Weller, S. Förster, Completely Miscible Nanocomposites, Angewandte Chemie International Edition, 50 (2011) 7811-7814.
[18] R. Shabnam, H. Ahmad, Hydrophobic poly(lauryl methacrylate)-coated magnetic nano-composite particles for removal of organic pollutants, Polymers for Advanced Technologies, 26 (2015) 408-413.
[19] Y. Liu, Y. Zhou, W. Nie, L. Song, P. Chen, Formation and surface properties of raspberry-like silica particles: effect of molecular weight of the coating poly(methacrylic acid) brushes, Journal of Sol-Gel Science and Technology, 72 (2014) 122-129.
[20] C. Ge, A. Wang, H. Yin, Encapsulation of TiO2 particles with polystyrene and polymethyl acrylic acid and the pigmentary performances, Journal of Industrial and Engineering Chemistry, 18 (2012) 1384-1390.
[21] P.S. Bhosale, J. Chun, J.C. Berg, Electrophoretic mobility of poly(acrylic acid)-coated alumina particles, Journal of Colloid and Interface Science, 358 (2011) 123-128.

[22] L.M. Bronstein, E.V. Shtykova, A. Malyutin, J.C. Dyke, E. Gunn, X. Gao, B. Stein, P.V. Konarev, B. Dragnea, D.I. Svergun, Hydrophilization of Magnetic Nanoparticles with Modified Alternating Copolymers. Part 1: The Influence of the Grafting, The Journal of Physical Chemistry C, 114 (2010) 21900-21907.
[23] T.A. Grünewald, A. Lassenberger, P.D.J. van Oostrum, H. Rennhofer, R. Zirbs, B. Capone, I. Vonderhaid, H. Amenitsch, H.C. Lichtenegger, E. Reimhult, Core–Shell Structure of Monodisperse Poly(ethylene glycol)-Grafted Iron Oxide Nanoparticles Studied by Small-Angle X-ray Scattering, Chemistry of Materials, 27 (2015) 4763-4771.
[24] P.J. Kempen, A.S. Thakor, C. Zavaleta, S.S. Gambhir, R. Sinclair, A Scanning Transmission Electron Microscopy Approach to Analyzing Large Volumes of Tissue to Detect Nanoparticles, Microscopy and Microanalysis, 19 (2013) 1290-1297.
[25] U.S. Jeng, T.-L. Lin, C.-S. Tsao, C.-H. Lee, T. Canteenwala, L.Y. Wang, L.Y. Chiang, C.C. Han, Study of Aggregates of Fullerene-Based Ionomers in Aqueous Solutions Using Small Angle Neutron and X-ray Scattering, The Journal of Physical Chemistry B, 103 (1999) 1059-1063.
[26] T.L. Lin, U. Jeng, C.S. Tsao, W.J. Liu, T. Canteenwala, L.Y. Chiang, Effect of Arm Length on the Aggregation Structure of Fullerene-Based Star Ionomers, The Journal of Physical Chemistry B, 108 (2004) 14884-14888.
[27] J.-M. Lin, T.-L. Lin, U.S. Jeng, Z.-H. Huang, Y.-S. Huang, Aggregation structure of Alzheimer amyloid-[small beta](1-40) peptide with sodium dodecyl sulfate as revealed by small-angle X-ray and neutron scattering, Soft Matter, 5 (2009) 3913-3919.
[28] K. Butter, A. Hoell, A. Wiedenmann, A.V. Petukhov, G.-J. Vroege, Small-angle neutron and X-ray scattering of dispersions of oleic-acid-coated magnetic iron particles, Journal of Applied Crystallography, 37 (2004) 847-856.
[29] T. Schindler, M. Schmiele, T. Schmutzler, T. Kassar, D. Segets, W. Peukert, A. Radulescu, A. Kriele, R. Gilles, T. Unruh, A Combined SAXS/SANS Study for the in Situ Characterization of Ligand Shells on Small Nanoparticles: The Case of ZnO, Langmuir, 31 (2015) 10130-10136.
[30] A.-S. Robbes, F. Cousin, F. Meneau, C. Chevigny, D. Gigmes, J. Fresnais, R. Schweins, J. Jestin, Controlled grafted brushes of polystyrene on magnetic [gamma]-Fe2O3 nanoparticlesvianitroxide-mediated polymerization, Soft Matter, 8 (2012) 3407-3418.
[31] M.J.A. Hore, J. Ford, K. Ohno, R.J. Composto, B. Hammouda, Direct Measurements of Polymer Brush Conformation Using Small-Angle Neutron Scattering (SANS) from Highly Grafted Iron Oxide Nanoparticles in Homopolymer Melts, Macromolecules, 46 (2013) 9341-9348.
[32] R. Massart, E. Dubois, V. Cabuil, E. Hasmonay, Preparation and properties of monodisperse magnetic fluids, Journal of Magnetism and Magnetic Materials, 149 (1995) 1-5.
[33] J.F. Berret, O. Sandre, A. Mauger, Size Distribution of Superparamagnetic Particles Determined by Magnetic Sedimentation, Langmuir, 23 (2007) 2993-2999.
[34] S. Lefebure, E. Dubois, V. Cabuil, S. Neveu, R. Massart, Monodisperse magnetic nanoparticles: Preparation and dispersion in water and oils, Journal of Materials Research, 13 (1998) 2975-2981.
[35] A. Bee, R. Massart, S. Neveu, Synthesis of very fine maghemite particles, Journal of Magnetism and Magnetic Materials, 149 (1995) 6-9.
[36] A. Sehgal, Y. Lalatonne, J.-F. Berret, M. Morvan, Precipitation-redispersion of cerium oxide nanoparticles with poly(acrylic acid): Toward stable dispersions, Langmuir, 21 (2005) 9359-9364.
[37] M. Peng, L. Sun, L. Chen, G. Sun, B. Chen, C. Xie, Q. Xia, G. Yan, Q. Tian, C. Huang, B. Pang, Y. Zhang, Y. Wang, Y. Liu, W. Kang, J. Gong, A new small-angle neutron scattering spectrometer at China Mianyang research reactor, Nuclear Instruments and Methods in Physics Research Section A: Accelerators, Spectrometers, Detectors and Associated Equipment, 810 (2016) 63-67.
[38] R.H. Müller, C. Jacobs, O. Kayser, Nanosuspensions as particulate drug formulations in therapy, Advanced Drug Delivery Reviews, 47 (2001) 3-19.
[39] I. Breßler, J. Kohlbrecher, A.F. Thünemann, SASfit: a tool for small-angle scattering data analysis using a library of analytical expressions, Journal of Applied Crystallography, 48 (2015) 1587-1598.

Figure captions

Scheme 1. Representation of the coating process using positively charged bare NPs and negatively charged PAA oligomers. Synthesized γ-Fe_2O_3-PAA NPs exhibit negative charges at their surface at pH = 7.5.

Scheme 2. Left: Representation of the polymer coated NPs. Right: the sphere model used to analyze SANS data for the iron oxide composite materials. Here the core is shown in yellow and the shell (ΔR) is blue. The scattering length density ρ of D_2O, pure PAA shell and γ-Fe_2O_3 are 6.63×10^{10} cm^{-2}, 1.59×10^{10} cm^{-2} and 7.17×10^{10} cm^{-2} respectively.

Figure 1. Transmission electron micrographs of bare and coated NP1. (a) Bare NP1; (b) NP1 coated with PAA_{2K} (NP1-PAA_{2K}); (c) NP1 coated with PAA_{5K} (NP1-PAA_{5K}); (d) Median diameter of bare and coated NPs obtained from TEM.

Figures 2. SAXS data of γ-Fe_2O_3 nanoparticles suspensions. (a) NP1 without and with PAA coating. (b) NP2 without and with PAA coating. The continuous lines are best fits to log-normal size distribution of spherical particles.

Figures 3. SANS curves obtained from of (a) NP1 and their corresponding coated samples which are dispersed in D_2O; (b) NP2 and their corresponding coated samples. The continuous line is the best fit calculation using a log-normal distribution of bare NPs and a linear contrast profile of the organic shell for the coated NPs.

Tables

Table 1. *Size and zeta potentials of bare and coated NPs characterized from DLS*

Sample name	D_H (nm)	Polydispersity S_{DLS}	Hydrodynamic size of polymer coating (nm)	zeta potential (mv)
NP1	8.4	0.18	—	+ 19
NP1-PAA_{2K}	22.0	0.21	6.8	- 29
NP1-PAA_{5K}	28.0	0.25	9.8	- 33
NP2	20.2	0.25	—	+ 21
NP2-PAA_{2K}	34.0	0.23	6.9	- 32
NP2-PAA_{5K}	43.3	0.24	11.5	- 34

Table 2. *Results of SAXS and SANS analysis on bare and coated NPs*

Sample	Fitted core radius R_{SAXS} (nm)	Polydispersity S_{SAXS}	Fitted core radius R_{SANS} (nm)	Shell thickness $D_{shell\ SANS}$ (nm)
NP1	2.43 ± 0.02	0.31	2.56±0.01	-
NP1-PAA_{2K}	2.50 ± 0.02	0.35	-	1.246±0.002
NP1-PAA_{5K}	2.48 ± 0.02	0.30	-	1.320±0.002
NP2	3.92 ± 0.02	0.27	3.86±0.01	-
NP2-PAA_{2K}	3.91 ± 0.01	0.34	-	1.244±0.003
NP2-PAA_{5K}	4.40 ± 0.01	0.39	-	1.323±0.003

ACCEPTED MANUSCRIPT

Supporting Information

Thickness Determination of Ultrathin Poly(acrylic acid) Shell on γ-Fe_2O_3 Nanocore via Small-Angle Scattering

Huailiang Li, Kunzhou Wang, Xianguo Tuo, László Almósy, Qiang Tian, Guangai Sun, Mark Julian Henderson, Qintang Li, András Wacha, Jérémie Courtois and Minhao Yan**

Outline

S1 Microdiffraction of γ-Fe_2O_3 nanocrystals

Fig. S1 presents the electron diffraction pattern obtained by TEM of the iron oxide nanocrystals of the study. The pattern is characteristic of maghemite (γ-Fe_2O_3).

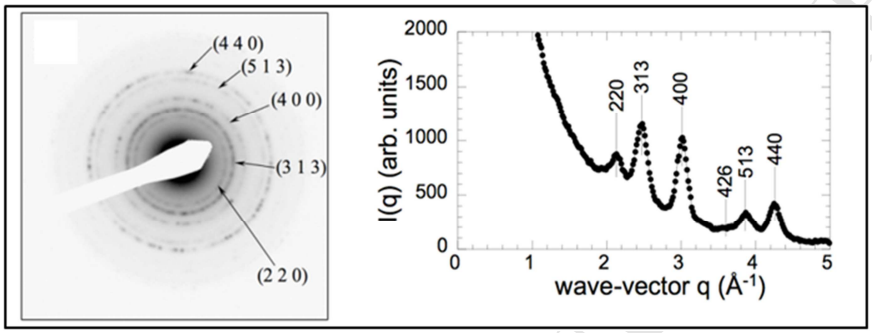

Fig. S1: *Microdiffraction curves of maghemite nanocrystals.*

S2 Vibrating Sample Magnetometry (VSM) analysis of the γ-Fe_2O_3 NPs

Vibrating sample magnetometry (VSM) measured the magnetization *versus* excitation *M(H)* of a liquid dispersion containing a volume fraction ϕ of magnetic material from the signal induced in detection coils when the sample is moved periodically in an applied magnetic field (via synchronous detection and with an appropriate calibration). Fig. S2 shows the evolution of the macroscopic magnetization *M(H)* of the polymer-coated maghemite nanocrystal. Here, $M_S = \phi m_S$, where ϕ is the volume fraction of maghemite and m_S is the specific magnetization of colloidal maghemite ($m_S = 3.5 \times 10^5$ A m^{-1}), which is lower than that of bulk maghemite due to some disorder of the magnetic moments located near the surface.

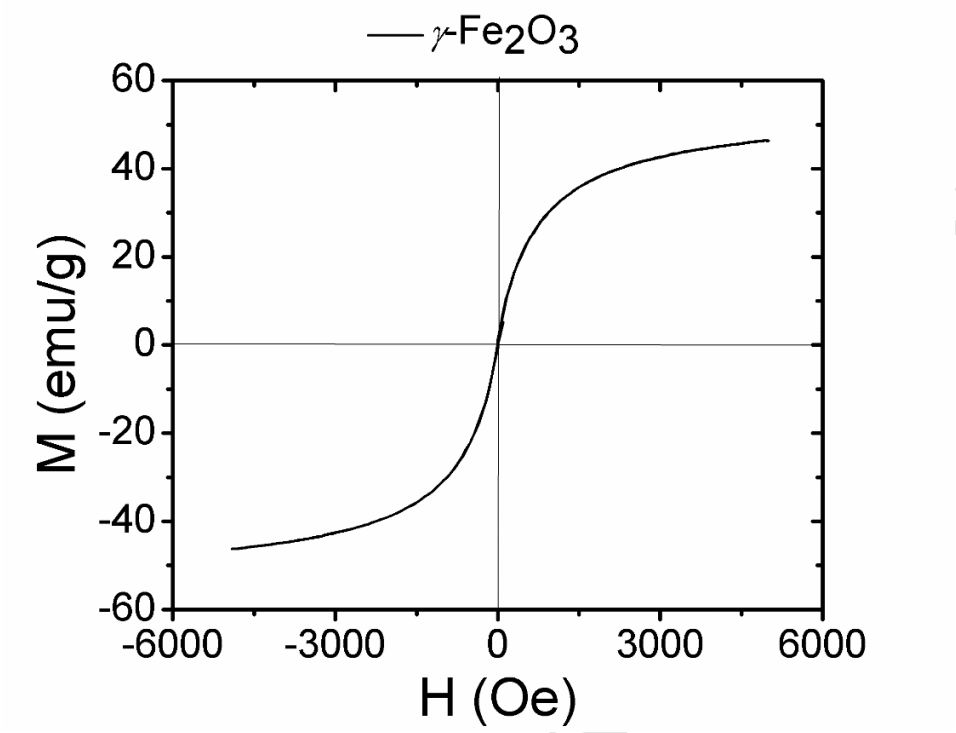

Fig. S2: *Magnetic field dependence of the macroscopic magnetization M(H) for γ-Fe_2O_3 NPs dispersions.*

S3 X-ray and neutron scattering length density

The neutron and X-ray scattering length densities ρ_N and ρ_X , for the materials within the different regions are presented in Table 1. The scattering length densities are calculated according to,

$$\rho_N = \frac{\sum_i^n b_{ci} \times D \times N_A}{M_W} \qquad \text{SI (1)}$$

where b_{ci} is the coherent scattering length of element *i* in a molecule; *D* is the physical density of the material; N_A is Avogadro's number and M_w is the molecular weight. The X-ray scattering length density ρ_X is related to physical density according to

$$\rho_X = \frac{\sum_i^n Z r_e \times D \times N_A}{M_W} \qquad \text{SI (2)}$$

where r_e is the classic electron radius, 2.81 x 10^{-13} cm, Z the atomic number of the i^{th} atom in the molecular volume.

Table S1 Estimated neutron and X-ray scattering length densities

Materials	ρ_N (Å^{-2})	ρ_X (Å^{-2})
PAA	1.51×10^{-6}	9.9×10^{-6}
γ-Fe_2O_3	7.17×10^{-6}	41.1×10^{-6}
H_2O	-0.56×10^{-6}	9.47×10^{-6}
D_2O	6.4×10^{-6}	9.37×10^{-6}

As shown in Table S1, one can see that, for SAXS technique, the contrast between γ-Fe_2O_3 and surrounding solvent (both H_2O and D_2O) is high, while the contrast between organic PAA and surrounding solvent (both H_2O and D_2O) is almost negligible. On the other hand, for SANS, γ-Fe_2O_3 core and PAA shell can be highlighted by choosing D_2O as solvent. Therefore for both SAXS and SANS experiments in the work, D_2O is the solvent of choice for both bare and coated NPs dispersions.

S4 Transmission Electron Microscopy (TEM) analysis of NPs

Probability distribution functions of size for the bare and coated NPs observed by TEM on a series of images are shown in Fig. S1.

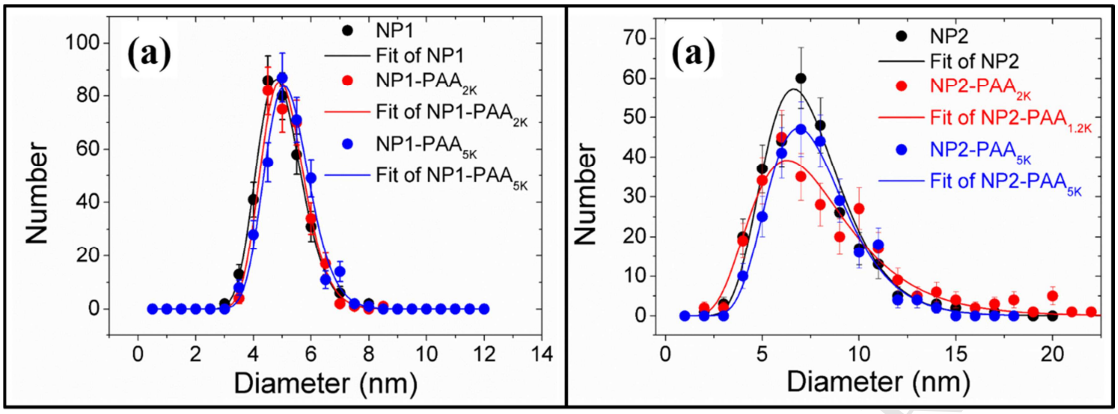

Figures. S1: *Probability distributions function of size for the* bare and coated NPs *superparamagnetic NPs. (a) bare and coated NP1 ; (b) bare and coated NP2. The continuous line was derived from a best-fit calculation using a log-normal distribution.*

The data are fitted using a log-normal function (equation SI (3)) with physical median diameter D_0^{TEM} and polydispersity s^{TEM} :

$$p(D) = \frac{1}{\sqrt{2\pi}(s^{TEM})D} \exp\left(-\frac{\ln^2(D/D_0^{TEM})}{2(s^{TEM})^2}\right) \qquad \text{SI (3)}$$

S5 TEM characterization of bare and coated NP2

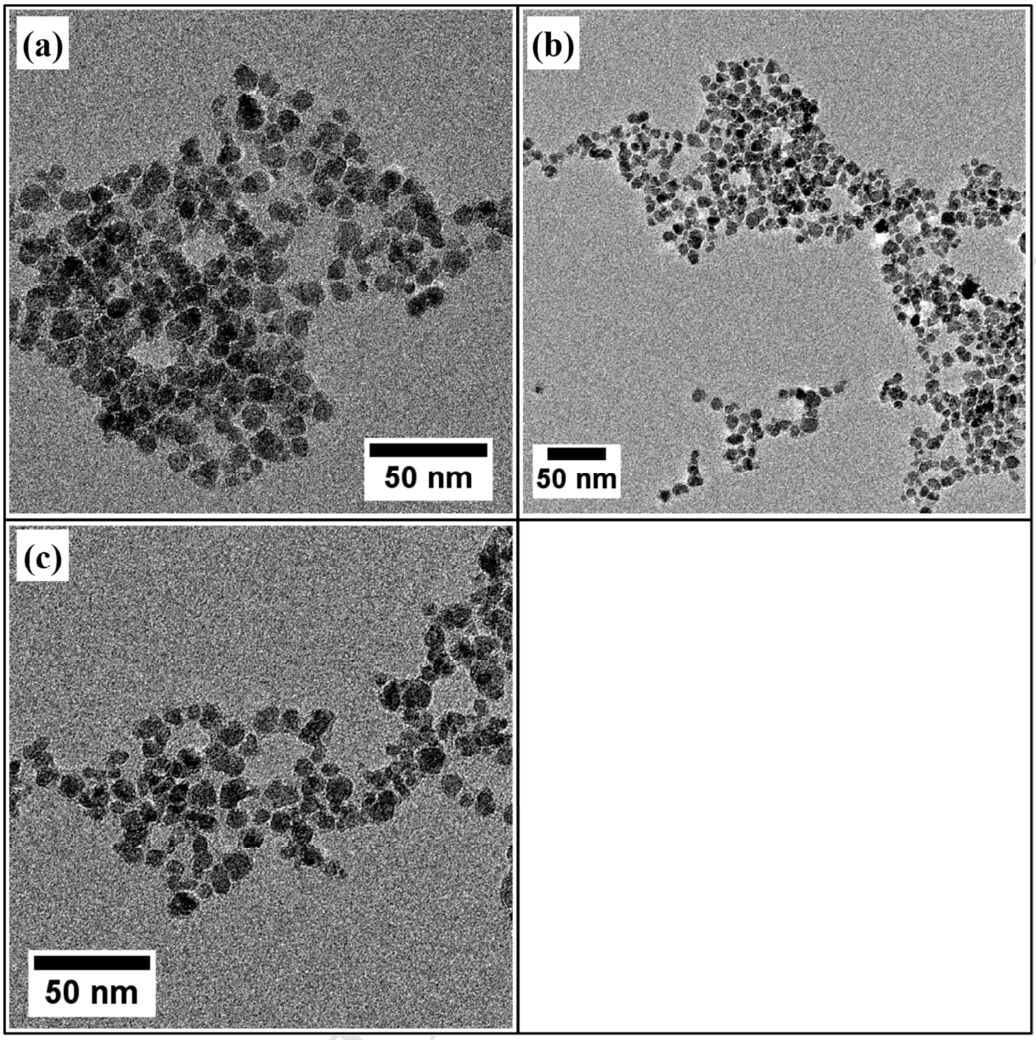

Figures S2. *Transmission electron micrographs of bare and coated NP2. (a): Bare NP2; (b) NP2 coated with PAA_{2K} (NP2-PAA_{2K}); (c) NP2 coated with PAA_{5K} (NP2-PAA_{5K}).*

ACCEPTED

S6 **Modeling of small-angle X-ray and neutron scattering scattering data**

The scattering of a dilute solution of core-shell particles can be written as the integral over particle size of the form factor of a core-shell particle. The size distribution is taken as log-normal, in agreement with the results of TEM observations.

$$f(R) = \frac{1}{\sigma R\sqrt{2\pi}} \exp[-\frac{1}{2\sigma^2}(\ln R - \ln R_0)^2] \qquad \text{SI (4)}$$

where σ is the variance, and R_0 is the median radius.

For the SAXS data, only the particle core is visible, and the core-shell form factor reduces to the form-factor of the spherical core:

$$F_{\text{core}}(q,R) = \frac{4\pi}{3} R^3 \frac{3[\sin qR - qR\cos(qR)]}{(qR)^3} \qquad \text{SI (5)}$$

In SANS measurement, the scattering of the polymer shell becomes visible, and is modeled as follows. As shown in Scheme 2, in the radial direction from the center of the particle, the contrast of scattering length densities is expressed as

$$\Delta\rho(r) = \begin{cases} \rho_{core} - \rho_{sol} & r < R \\ mr - mR + \rho_{shell} - \rho_{sol} & R < r < R + \Delta R \\ 0 & r > R + \Delta R \end{cases} \qquad \text{SI (6)}$$

where ρ_{core} and ρ_{shell} are the scattering length density of Fe_2O_3 and pure PAA, ΔR is the maximal thickness of the PAA shell, and $m = (\rho_{sol} - \rho_{shell})/\Delta R$.

The form factor of the core-shell particle is expressed as :

$$P_{core\text{-}shell}(q,R) = \left[\begin{array}{l} (\rho_{core} - \rho_{shell} + mR)F_{core}(q,R) + (\rho_{shell} - \rho_{sol} - mR)F_{core}(q,R+\Delta R) \\ +mF_{shell}(q,R+\Delta R) - mF_{shell}(q,R) \end{array} \right]^2$$

SI (7)

where $F_{core}(q, R)$ and $F_{shell}(q, R)$ are the scattering amplitude of Fe_2O_3 core and PAA shell, respectively, and

$$F_{\text{shell}}(q,R) = 4\pi R^4 \frac{2\cos(qR) + 2qR\sin(qR) - (qR)^2\cos(qR)}{(qR)^4} \qquad \text{SI (8)}$$

The final fitting equation is written as

$$I(q) = K\int_0^\infty (\frac{4\pi}{3}R^3)^2 f(R) P_{core\_shell}(q,\ R)dR \qquad \text{SI (9)}$$

In the fitting procedure, this equation is convoluted with the instrumental resolution function.

ACCEPTED MANUSCRIPT

ACCEPTED MANUSCRIPT

- Polymer coated γ-Fe_2O_3 nanoparticles are highly stable in aqueous media.
- "Stealth" polymeric coatings cannot be easily and accurately detected.
- SANS offers in situ structural information on core/shell structures.
- The methods are applicable for nano-composite systems with organic shells.

ACCEPTED MANUSCRIPT